Research article

Geoenergy

https://doi.org/10.1144/geoenergy2024-023 | Vol. 3 | 2025 | geoenergy2024-023

Diagenetic evolution of the Bunter Sandstone Formation and its controls on reservoir quality: implications for CO_2 injectivity and storage

Jeremy C. Rushton*, Sarah Hannis, Jonathan Pearce, John Williams and Antoni E. Milodowski

British Geological Survey, Nicker Hill, Keyworth, Nottingham NG12 5GG, UK
JCR, 0000-0001-5931-7537; JW, 0000-0003-0177-9848; AEM, 0000-0002-5141-5615
* Correspondence: jere1@bgs.ac.uk

Abstract: The Bunter Sandstone Formation (BSF) is a target reservoir for the storage of CO_2 in the UK Southern North Sea (UKSNS). Previous industry studies highlighted diagenetic features that influence fluid flow in the BSF but failed to identify the controls and patterns of regional diagenesis that are now needed to inform more accurate prediction of porosity distribution and connectivity for CO_2 storage. This study presents a regional diagenetic model from the petrographical analysis of 78 samples from 12 wells in the northern UKSNS. Diagenetic cements (carbonates, sulfates and halite) are common. Most are early and episodic, patchy at local and regional scales, with periods of replacement and dissolution. Consequential fine-scale heterogeneous compaction textures are unrelated to current or maximum burial depths. Calcrete and dolocrete layers, associated with the formation of displacive eodiagenetic carbonate nodules, form discontinuous millimetre- to metre-thick vertical flow barriers. Halite and anhydrite are developed preferentially in coarser-grained sandstones, resulting in the 'reservoir quality inversion' noted in previous studies. There is abundant evidence for local, late mobilization and dissolution of halite and anhydrite, observed to preferentially affect samples from depths above *c.*1400 m, restoring some zones to good porosity. Additional high-density sampling and petrography is recommended, however, to provide the predictability required for CO_2 storage.

Received 18 July 2024; **revised** 15 November 2024; **accepted** 2 December 2024

The Bunter Sandstone Formation (BSF) is a saline aquifer target for CO_2 storage in the UK Southern North Sea (UKSNS). Several carbon storage licences have been issued in the UKSNS to date where the BSF represents either the primary, or a potential secondary, storage reservoir (Fig. 1). The BSF is a Triassic sheet-sand complex averaging more than 200 m in thickness, which has been gently folded into a series of large anticlinal structures, many with periclinal forms (Cameron *et al.* 1992). It is these structures that are considered as some of the most prospective sites for CO_2 storage in the UKSNS (Holloway *et al.* 2006; Noy *et al.* 2012; Hollinsworth *et al.* 2022). Although gas production from the BSF has now ceased, a small number of these closures contained natural gas and were extensively investigated during gas exploration and development activities (Bifani 1986; Ketter 1991; Ritchie and Pratsides 1993). While the CO_2 storage capacity of the saline water-bearing parts of the formation far exceeds that of the limited number of BSF gas fields (Gammer *et al.* 2011; Bentham *et al.* 2014), fewer data are generally available from which to attain a detailed understanding of reservoir property distributions. Most wells in the region were drilled to explore and to develop deeper gas-bearing reservoirs of Permian and Carboniferous age. As a result, core sampling in the BSF is concentrated in the gas fields, and the distribution and coverage of cored materials is relatively sparse (Hollinsworth *et al.* 2022). A dedicated CO_2 storage appraisal well was drilled in 2013 to de-risk aspects of the Endurance site (42/25d-3), from which *c.* 137 m of core was retrieved from both the reservoir and cap-rock section (Furnival *et al.* 2014; Gluyas and Bagudu 2020).

Previous studies have highlighted the presence of small-scale sedimentary and diagenetic features that can potentially influence fluid flow in the BSF (Bifani 1986; Ketter 1991; Ritchie and Pratsides 1993). Additionally, a regional-scale diagenetic feature thought to be related to pervasive halite cementation is identifiable on seismic reflection data across part of the basin (Furnival *et al.* 2014; Hollinsworth *et al.* 2022). The occlusion of porosity by halite cement may therefore play an important role in planning for future CO_2 storage operations in the BSF. Modelling studies have highlighted the potential impact of local heterogeneities on CO_2 migration, storage efficiency and capacity (Williams *et al.* 2013). At the regional scale, studies of pressure propagation in response to CO_2 storage suggest that any injection activities may be likely to affect the formation pressures over potentially large areas well beyond the storage location (Noy *et al.* 2012; Agada *et al.* 2017). These studies highlight the need to develop a comprehensive understanding of the regional pattern of diagenetic alteration influencing reservoir properties. Consequently, a petrographical study was conducted by the British Geological Survey (Rushton *et al.* 2023), examining 78 BSF samples from 12 wells (Fig. 1). In this paper we additionally consider the potential implications of diagenesis on CO_2 storage in the BSF, at both local and regional scales.

Geological history

The UKSNS lies at the western extent of the Southern Permian Basin, a depositional centre from the early Permian until the early Jurassic (Cameron *et al.* 1992; Doornenbal and Stevenson 2010). Underlain by eroded Carboniferous rocks, basin fill commenced with the deposition of aeolian sands and desert lake sediments of the Lower Permian Rotliegend Group. The Rotliegend Group includes the Leman Sandstone Formation, which is the most prolific gas reservoir in the Southern North Sea (Fig. 2). Sea-level fluctuations coupled with continued subsidence in the Late Permian resulted in the deposition of thick carbonate–evaporite cycles, ascribed to the

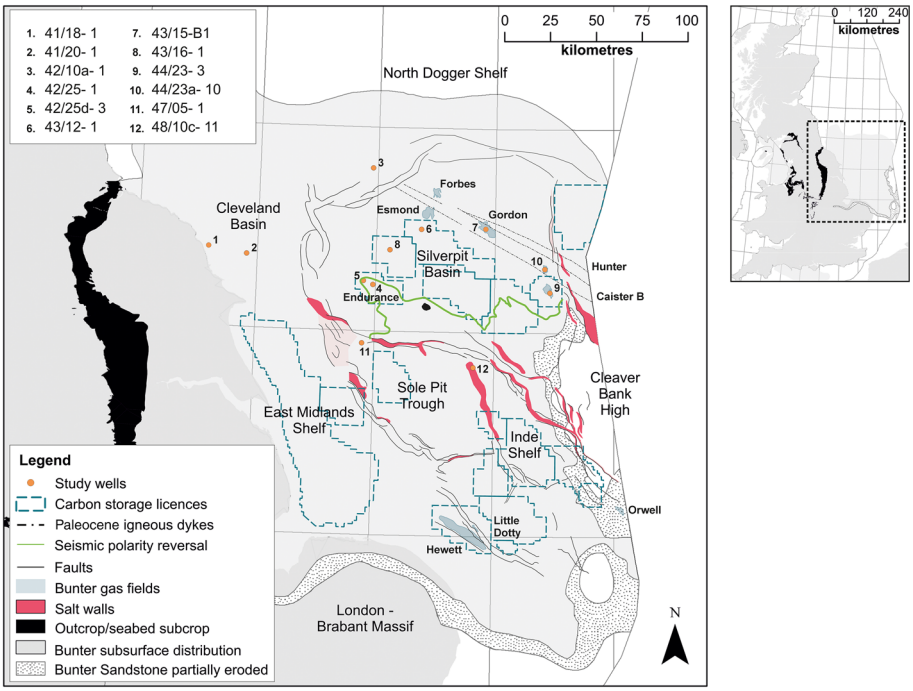

Fig. 1. BSF extent, key geological features and the locations of petrographical samples.Source: BSF extent after Cameron *et al.* (1992). The offshore quadrant, gas field and carbon storage licence linework contains information provided by the North Sea Transition Authority and/or other third parties.

Zechstein Group (Johnson *et al.* 1994). A return to continental conditions during the earliest Triassic resulted in the deposition of the Bacton Group, which comprises the Bunter Shale Formation and the overlying BSF.

In the UKSNS, the BSF was deposited on an extensive low-topography plain under arid to semi-arid conditions, with fluvial sediments predominantly derived from the west and SW via the Triassic river drainage system, and contributions of aeolian-derived/reworked material from the east (cf. McKie and Williams 2009; Newell 2018). More than 350 m of sandstones are preserved in the Sole Pit Trough (Cameron *et al.* 1992; Ruffell and Hounslow 2006). The laterally equivalent unit in countries to the east of the UK can be subdivided into seven upward-fining tectonostratigraphic units, each comprising a system of parasequences related to Milankovitch climatic cycles (Geluk and Röhling 1997; Geluk 2005). The major tectonostratigraphic units identified by Geluk and Röhling (1997) in the Dutch sector can only partially be identified in the UKSNS because the BSF is highly sand-prone and there is an absence of distinct marker horizons (Cameron *et al.* 1992; Ruffell and Hounslow 2006). At a more local scale, gas field studies have defined up to seven locally correlatable zones based on rock properties and depositional environments inferred from core studies (Ketter 1991; Ritchie and Pratsides 1993). In a regional context, it is likely that some subdivisions represent minor hiatuses, unconformities or changes in sediment transport, as have been identified in The Netherlands (Geluk and Röhling 1997).

The top of the BSF is defined by the Hardegsen Unconformity, which is evident as an angular unconformity towards the northern extent of the BSF and is described as a tectono-eustatic event (Ziegler 1982). The Hardegsen Unconformity separates the BSF from the top seals of the overlying Haisborough Group. A thin playa mudstone unit directly overlies the BSF, which is laterally equivalent to the Solling Formation in The Netherlands. Subsequently, marine incursions led to deposition of the overlying Röt Halite Member. The remaining Triassic sequence comprises a thick mudstone and carbonate sequence punctuated by local evaporites.

Towards the end of the Jurassic through to the Cretaceous, uplift and erosion occurred, particularly along the Sole Pit Trough (Fig. 1) which was uplifted to create the Sole Pit High with up to 2 km of erosion by the late Cretaceous (Bulat and Stoker 1987; Van Hoorn 1987; Japsen 2000). The Late Cimmerian Unconformity marks the base of the Cretaceous, and cuts down through the Jurassic and Triassic into the BSF over the Cleaver Bank High in the eastern part of the UKSNS. Although the majority of petrographical samples available to this study were collected to the north of the inversion axis, tectonics associated with inversion of the Sole Pit Trough may have influenced fluid flow and diagenetic events in the BSF.

For most of the sample locations in the study area, it is thought that maximum burial was reached immediately prior to the Neogene (Cenozoic uplift) period of uplift and erosion that exhumed the BSF at the westernmost extent of the Southern Permian Basin. The degree of this uplift and erosion reduces from a maximum in the East Midlands Shelf of *c.* 1 km towards the UK–Netherlands median line, where it is estimated at 0.5 km (Japsen 2000).

These regional tectonic trends have been overprinted by halokinesis, which was initiated during the Mid–Late Triassic, by mobilization of the Zechstein evaporites during basin extension. This was largely controlled by the distribution of underlying (pre-Permian) faulting and salt thickness (Underhill 2009). This halokinesis resulted in folding of the BSF and overlying sediments into the anticlinal structures currently of interest for CO_2 storage. The region also became compartmentalized by major fault zones and salt walls, primarily along the Dowsing Graben System and North Dogger Fault Zone (Smith *et al.* 2011; Noy *et al.* 2012). Exposure of the study area at surface, as part of Doggerland, occurred several times during Pleistocene glacial maxima (Coles 1998), with parts of Dogger Bank still exposed as recently as 8200 years BP (Walker *et al.* 2020). Consequently, meteoric water incursion will have affected the study area, including the potential for flushing of shallow and deep aquifers. The Silverpit BSF subcrop (Fig. 1) provided one direct pathway for meteoric waters to the BSF.

Further background details on the stratigraphy, structure and petroleum systems of the SNS are described by Cameron *et al.* (1992) and Underhill (2003).

Previous petrographical studies

The few published petrographical studies of BSF diagenesis are restricted to single wells, fields or geographically constrained areas.

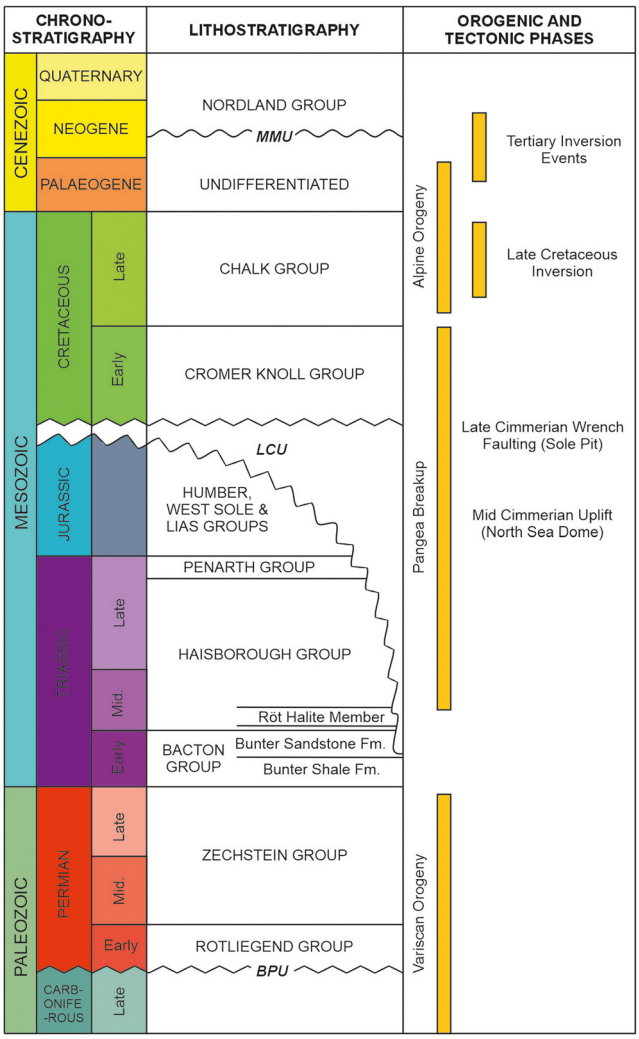

Fig. 2. Stratigraphic column with key tectonic events. MMU, Mid-Miocene Unconformity; LCU, Late Cimmerian Unconformity; BPU, Base Permian Unconformity.

All studies from the UK and Dutch sectors have reported the presence of common to abundant diagenetic cements, notably halite with anhydrite and carbonates. These studies generally agree that porosity and permeability are controlled both by original depositional texture and subsequent diagenesis, with the former having a particularly strong control on the distribution of the latter. Timings and mechanisms have been proposed for selected UK sites (Poroperm-Geochem Ltd 1987; Blackbourn and Robertson 2014) and for study areas in neighbouring countries (Laier and Nielsen 1989; Purvis and Okkerman 1996). Prior to the petrographical study summarized here, a regional understanding of the diagenetic history and its influence on reservoir quality has not been published for the UKSNS.

In studies of UKSNS gas fields, Ritchie and Pratsides (1993) postulated that halite cementation was inhibited in the gas leg, while Ketter (1991) noted that coarser-grained sandstones had reduced porosities due to preferential cementation. Inversion of reservoir quality is also observed in some wells in The Netherlands sector (Purvis and Okkerman 1996). The distribution, timing and origins of the main cements, particularly halite, have been a major point of discussion and speculation in these studies. Halite cementation is reported as both an early- and a late-stage diagenetic event, resulting from saline brine expulsion from the underlying Zechstein due to gypsum–anhydrite transformation and halokinesis during Alpine tectonism, respectively. Earlier halite derived from overlying Triassic evaporites during Cimmerian uplift has also been proposed (Poroperm-Geochem Ltd 1987). Van Bergen and de Leeuw (2001) postulated that halite cementation resulted from temperature gradient distortion around salt domes. This would have resulted from the removal of Permian evaporites between salt diapirs during halokinesis, which enabled the vertical migration of overpressured and saturated Permian brines from which halite precipitated when reaching lower temperatures in the BSF adjacent to the salt domes.

In contrast, Muir *et al.* (1994) concluded that halite cements formed in the shallow subsurface from highly saline groundwater. They describe *c.* 3 m fining-upward cycles with calcrete towards the base and increasing anhydrite and halite towards the top of each cycle. Purvis and Okkerman (1996) determined from $\delta^{34}S$ isotopic values (+4.2 to +12.1‰ CDT) that the Zechstein was the most likely source of the anhydrite. Furthermore, the exclusion of other cements in pores filled with halite indicated that the halite was early, derived from saline brines produced from Zechstein halite, dissolved by liquids evolved during the dewatering of Zechstein gypsum.

A detailed diagenetic study of the Endurance structure noted the absence of patchy early dolomite and anhydrite cements that had been identified in surrounding wells (Blackbourn and Robertson 2014). These were inferred to have been subsequently partially removed by thermohaline convection and potentially some meteoric influx from a nearby outcrop. Relative to typical porosity–depth trends, the BSF at Endurance has a higher porosity than expected that has been attributed to late-stage halite dissolution. The zone of higher porosities, particularly in the upper part of the BSF, can be distinguished from surrounding wells exhibiting enhanced cementation by a regionally extensive polarity phase reversal observed on seismic data (Furnival *et al.* 2014; BP 2021*a*; Hollinsworth *et al.* 2022). Blackbourn and Robertson (2014) also noted the presence of a metre-scale thickness calcareous interval across the structure, which they interpret to comprise reworked ooids derived from the underlying Bunter Shale Formation.

Samples and methods

New samples were prepared from hydrocarbon industry borehole materials (mostly legacy) stored at the British Geological Survey's National Geological Repository, with a total of 78 samples from the BSF taken from 12 wells across the UKSNS (Fig. 1; Table 1). All samples were taken from drill core material other than samples from well 47/05-1, which were collected from cuttings. The bulk of the core material sampled for the study displayed the red colour characteristic of the BSF and onshore equivalent Sherwood Sandstone Group. The 'bleaching' (i.e. absence of red colour) also associated with these rocks was rarely observed (mostly as

Table 1. Distribution of samples by well and position within the BSF

Well	Number of samples	Sample interval	
		Upper Volpriehausen	Lower Volpriehausen
41/18-1	2	2	
41/20-1	2	2	
42/10a-1	2		2
42/25-1	4	4	
42/25d-3	10	10	
43/12-1	5	2	3
43/15-B1	2	2	
43/16-1	3	3	
44/23-3	18	15	3
44/23a-10	15	11	4
47/05-1[#]	3	1	2
48/10c-11	12	5	7
Total	**78**	**57**	**21**

Note that samples from well 47/05-1 were taken from cuttings rather than core.

spotting), and so was therefore not specifically examined in this study. Table 1 divides the BSF in the study area into two distinct units based on petrophysical characteristics. An Upper Volpriehausen unit is approximately equivalent to the Volpriehausen Clay–Siltstone Member identified in The Netherlands nomenclature, while a Lower Volpriehausen unit approximates to the Lower Volpriehausen Sandstone Member (Table 2). The younger Detfurth and Hardegsen formations are largely absent from the study area due to erosion beneath the Hardegsen Unconformity. Sampling is biased stratigraphically to the middle of the Upper Volpriehausen and the top of the Lower Volpriehausen, and geographically to wells in UK Quadrant 44 (Table 1).

Polished thin sections were examined using optical microscopy, high-resolution backscattered electron (BSE) imaging scanning electron microscopy (SEM), with mineral identification aided by qualitative energy-dispersive X-ray (EDX) microanalysis, optical cold-cathodoluminescence (CL) microscopy and SEM cathodoluminescence imaging (SEM-CL). A selection of sections was additionally analysed by automated quantitative mineralogy (AQM) using Zeiss' Mineralogic phase-mapping software (V1.6.2). For this same group of samples, quantitative porosity was determined using petrographical image analysis (PIA). Pore surfaces were examined by SEM secondary electron (SE) imaging.

Minus-cement porosity (Rosenfeld 1949) was determined for a subset of samples to inform the roles of compaction and diagenetic cementation in porosity evolution, specifically with respect to the relative timing of cementation events against burial and inversion. Although there are inherent complications in the application of this approach (as summarized by Paxton *et al.* 2002), it provides a useful indication of the compactional state. Secondary porosity and grain-replacive cement volumes were additionally derived by point counting.

Results

Summary of petrographical observations

The diagenetic characteristics most relevant to the controls on porosity and permeability distribution in the BSF are summarized below. The sandstone samples varied between quartz arenites, subfeldspathic arenites and sublithic arenites (after Pettijohn *et al.* 1987), and are notable for commonly having high feldspar contents (K-feldspar and plagioclase (mostly albite): Table 3). The sandstones are typically very fine–medium grained, with some coarse grained, commonly laminated with parallel-bedding and low-angle cross-bedding, and locally evident ripple lamination. Some centimetre-scale beds are upwards fining and some bed bases are erosive. The degree of dissolution of diagenetic cements and of framework grains is variable across the study area. Observations are consistent with previous studies that suggest the BSF is dominated by fluvial/sheetflood depositional environments within arid to semi-arid continental conditions (Bifani 1986; Ritchie and Pratsides 1993; Purvis and Okkerman 1996; McKie and Williams 2009). A limited reworked aeolian input is inferred from the presence of notably well-rounded coarse sand grains; which increase in abundance towards the east, and towards the top of the Lower Volpriehausen, and in the base and middle of the Upper Volpriehausen. Identification of pedogenic textures (e.g. clay infiltration and calcrete fabrics) is consistent with a model where periods of quiescence are punctuated by episodes of fluvial activity arising from occasional and heavy precipitation events in the headwater regions.

Following deposition, fabrics developed are typical of eodiagenesis in hot, semi-arid environments (cf. Walker *et al.* 1978) and have been previously described for both offshore (e.g. Muir *et al.* 1994 and references therein) and onshore (cf. Plant *et al.* 1999; Monaghan *et al.* 2012 and references therein). Early calcite and dolomite sand-sized spheroidal nodules have been commonly observed, particularly in the central to eastern parts of the study area, typically forming carbonate nodules with cores and multiple growth bands defined by hematitic clay films (Fig. 3a, b). Their subsurface formation is supported by radial crystal structures and sand grains included within their growth structures. No stratigraphic control was discernible for the distribution of these carbonate nodules. Nodules showing evidence of partial fragmentation were noted to be more abundant in the Lower Volpriehausen, which is interpreted to have been deposited in a higher energy environment than the Upper Volpriehausen. Carbonate nodules are also abundant in thin calcrete and dolocrete horizons developed in finer-grained laminations, indicating pedogenic carbonate formation. The commonly associated localized 'expanded' framework texture indicates displacive carbonate growth in the sediment under minimal overburden (Fig. 3b). These various features demonstrate that the nodules have formed in the surface and near-surface, potentially with several periods of formation, reworking and local redeposition (Rushton *et al.* 2023). It seems likely that these nodules correspond to the 'reworked ooids' identified by other authors (Blackbourn and Robertson 2014), since they superficially have ooid-like forms. Our observations show that whilst some have entirely detrital origins (implicit in the ooid descriptor), most have eodiagenetic and mixed detrital-eodiagenetic origins. We use the term 'nodule' to include all types.

Early anhydrite as nodular cement patches enclosing 'floating' detrital grains (Fig. 3c) was generally observed to post-date the eodiagenetic nodular carbonate. The local presence of early gypsum is inferred from rare 'desert rose' forms pseudomorphed by anhydrite. These early sulfate precipitates are widespread across the basin and are typical of sabkha environments (cf. Testa and Lugli 2000 and references therein; Warren 2006). A common to abundant weakly ferromanganoan calcite formed during early diagenesis, occluding intergranular pores, and nucleated on the carbonate nodules. Its composition is an indication of pore fluids becoming more reducing. Much of this calcite has formed displacively (particularly in calcrete horizons: Fig. 3b), indicating that it developed under near-surface, low-overburden conditions. However, some of the calcite is a pore-filling cement with no grain-displacive aspect, so has formed under

Table 2. Stratigraphic correlation showing relative relationships between the BSF nomenclature used in the UKSNS (Johnson *et al.* 1994) and The Netherlands (as summarized by Geluk and Röhling 1997)

UKSNS		The Netherlands		
Group	Formation	Group	Formation	Member
Bacton Group	Bunter Sandstone	Lower Germanic Trias	Hardegsen	
			Detfurth	Detfurth Claystone
				Lower Detfurth Sandstone
			Volpriehausen	Volpriehausen Clay–Siltstone
				Lower Volpriehausen Sandstone

Table 3. Modal analysis results from AQM and point counting, including minus-cement quantification, and compaction-model derived porosities at current and maximum burial

Well	Depth (m)	Sample number	Area analysed for PIA and AQM (mm^2)	Porosity from PIA	Normalized modal areas (%), excluding porosity, from AQM												Porosity = secondary	Cement = framework grains	Minus-cement porosity (%)	Theoretical porosity at the current depth†	Maximum burial (m)*	Theoretical porosity at maximum burial depth†	Maximum burial pre- or post-Chalk*	Stratigraphy (Volpriehausen)	Gas (G)/ water (W) leg
					Quartz	K-feldspar	Plagioclase	Calcite	Dolomite	Anhydrite	Barite	Halite	Matrix/ grain-coating clays	Micas	Kaolinite	Accessories									
41/18-1	511.0	SSK16097	97	13.6	56.1	8.4	17.5	Tr	7.5	0.6		0.4	8.4	0.2		0.8	Tr	3.8	17.8	38.4	2764	23.6	Pre	Upper	W
42/25-1	1137.3	SSK7150	89	15.5	44.4	10.6	13.9	11.3	3.1	0.1	Tr	Tr	15.1	1.19		0.38	4.3	2.8	21.3	34.3	2133	27.7	Pre	Upper	W
	1142.5	SSK7151	108	13.8	41.8	7.6	9.2	28.9	3.2	0.5	0.1	Tr	7.8	0.4		0.5	Tr	21.4	23.7	34.3	2138	27.7	Pre	Upper	W
43/12-1	1388.5	SSK16098	170	1.9	38.1	7.0	4.9	Tr	10.3	7.5	Tr	27.1	3.7	0.1		0.2	Tr	11.1	35.8	32.6	2287	26.7	Post	Upper	W
	1391.9	SSK16099	129	27.6	50.1	9.1	21.9	0.1	4.4	0.1			1.2	11.3	0.5	1.3	Tr	2.2	30.4	32.6	2290	26.7	Post	Upper	W
	1428.8	SSK16101	199	3.0	43.0	9.6	2.7	12.5	Tr	Tr	0.2	27.3	3.4	Tr		0.2	3.0	6.8	33.2	32.4	2327	26.4	Post	Lower	W
44/23-3	1374.8	SSK7137 sandstone	16	21.9	42.6	7.5	11.0	0.1	24.2	4.1			8.7	0.1	0.4	0.6	Tr	21.8	29.1	32.7	1716	30.5	Post	Upper	G
	1431.0	SSK7148	60	11.5	49.0	9.3	6.3	Tr	3.2	23.4	Tr	Tr	8.1	0.1	Tr	0.5	Tr	7.2	28.6	32.4	1772	30.1	Post	Upper	G
	1442.5	SSK7149A	171	22.5	58.2	16	5.4	Tr	2.3	12	Tr		5.8	Tr	Tr	0.1	1.0	2.3	30.3	32.3	1784	30.0	Post	Lower	W
44/23a-10	1855.3	SSK7142	200	Tr	33.8	6.2	10.3	Tr	15.5	8.2	0.1	19.0	6.3	0.1	0.1	0.5		13.7	29.1	29.6	2095	28.0	Post	Upper	G
	1918.2	SSK7134	115	11.2	64.4	9.1	1.6	Tr	0.1	0.4		21.6	2.7	Tr	0.1	0.1	0.5	0.5	30.0	29.1	2158	27.6	Post	Lower	W
	1921.6	SSK7135	123	22.6	56.0	14.9	3.2	19.5	0.9	Tr	Tr	0.5	4.8	Tr	Tr	0.1	1.0	7.8	32.3	29.1	2161	27.5	Post	Lower	W
48/10c-11	2016.6	SSK16116	122	7.0	21.1	2.3	3.0	3.6	58.7	Tr		1.2	9.1	0.2		0.6	6.0	>20	N/A	28.5	3297	20.0	Equal	Upper	W
	2080.9	SSK16110	167	2.0	62.6	5.2	0.3	2.4		0.9		26.8	1.6	Tr		0.1	2.0	2.3	27.3	28.1	3362	19.6	Equal	Lower	W
	2100.7	SSK16111	295	16.8	53.1	12.9	5.3	14.2	0.1	0.1	0.1	6.0	7.5	0.3		0.4	Tr	7.4	27.9	27.9	3381	19.5	Equal	Lower	W

*From Bulat and Stoker (1987); †from Ramm and Bjørlykke (1994); Tr, trace; N/A, not applicable as the sample is a dolocrete and the value of minus-cement porosity could not be quantified reliably.

significant overburden and therefore after the onset of burial. This shows that this period of calcite formation extended from the eodiagenetic into the mesodiagenetic regime.

Carbonate nodules have been variably recrystallized to coarser microsparite and microdolosparite, and some have been replaced by later (mesodiagenetic) ferroan dolomite (Fig. 3b), ankerite, ferroan calcite and anhydrite. Microcrystalline to micritic dolomite is a common cement in the mudstone and siltstone laminae.

During further burial, minor to trace euhedral K-feldspar (early mesodiagenetic: Fig. 4), quartz and albite overgrowths develop. Minor dissolution of early dolomite is followed by the formation of later widespread compositionally zoned dolomite that becomes increasingly iron-rich to form ankerite in outer zones. This dolomite–ankerite locally replaces eodiagenetic dolomite and fills secondary porosity after feldspar and lithic clast dissolution, indicating that it formed relatively early during mesodiagenesis. A further period of anhydrite formation has resulted in poikilotopic cements (Fig. 3c), which locally enclose and partially replace the eodiagenetic carbonates (including nodules), and has also locally partially replaced silicate framework grains. This anhydrite has infilled compaction-induced fractures, indicating that it formed after significant burial compaction, and locally displays the notched and embayed margins that show it has been subject to dissolution (Fig. 3c). Notably, compactional fabrics are similar within the still-cemented parts of the sandstone with rejuvenated (post-dissolution) porosity (Fig. 3c, d).

Halite is a major cement in sandstones of the BSF, occurring as poikilotopic, pore-filling cements. This cement fills compaction-induced grain fractures (Fig. 3e) and has also occluded intragranular micropores associated with some eodiagenetic nodules (Fig. 3e). Relict hematitic rims within poikilotopic halite indicate complete replacement of some carbonate nodules. It encloses, and therefore post-dates, the later anhydrite cement. As the anhydrite crystals have euhedral margins, the enclosure is interpreted to be largely passive, although there is local evidence for dissolution of anhydrite prior to, or during, halite emplacement. It is typically most developed in coarser-grained laminations (Fig. 3f), where it can occlude much of the secondary and remaining primary porosity. These observations show that halite is a mid–late mesodiagenetic phase.

Subsequently, some of this halite experienced minor dissolution (Fig. 3e). It is recognized that due to the legacy nature of the core samples, some of this dissolution could have occurred during coring and subsequent handling. However, textures developed on a more widespread scale are more likely to represent *in situ* halite dissolution. For example, significant porosity is present in specific laminations of an otherwise fully cemented sandstone sample with the porosity-exposed halite having dissolution textures (notches, embayments) and being present in only the narrowest pores. In summary, both halite cementation and dissolution are partly controlled by detrital grain sizes. Halite dissolution and reprecipitation is also identifiable in some millimetre-scale fractures.

Late diagenesis also resulted in the alteration of feldspar and felsic lithic grains with trace formation of authigenic kaolinite. Late-stage ferromanganoan calcite forms a minor pore-filling cement, with its distribution predominantly confined to primary and secondary porosity after anhydrite and halite dissolution, and enclosing kaolinite. Observed traces of fibrous illite are poorly preserved in open porosity in some sandstones. Potentially, this may have been more significant (as evident from some onshore wells) but in the absence of any specialized core preservation it is unlikely to be preserved in these legacy core samples (Milodowski *et al.* 1987). Finally, barite forms trace to minor late-stage, poikilotopic intergranular cement in the Upper Volpriehausen in some wells.

Recognition of primary porosity is complicated by the presence of extensive pedogenic and eodiagenetic carbonate and sulfate nodules and cements, and their subsequent recrystallization and

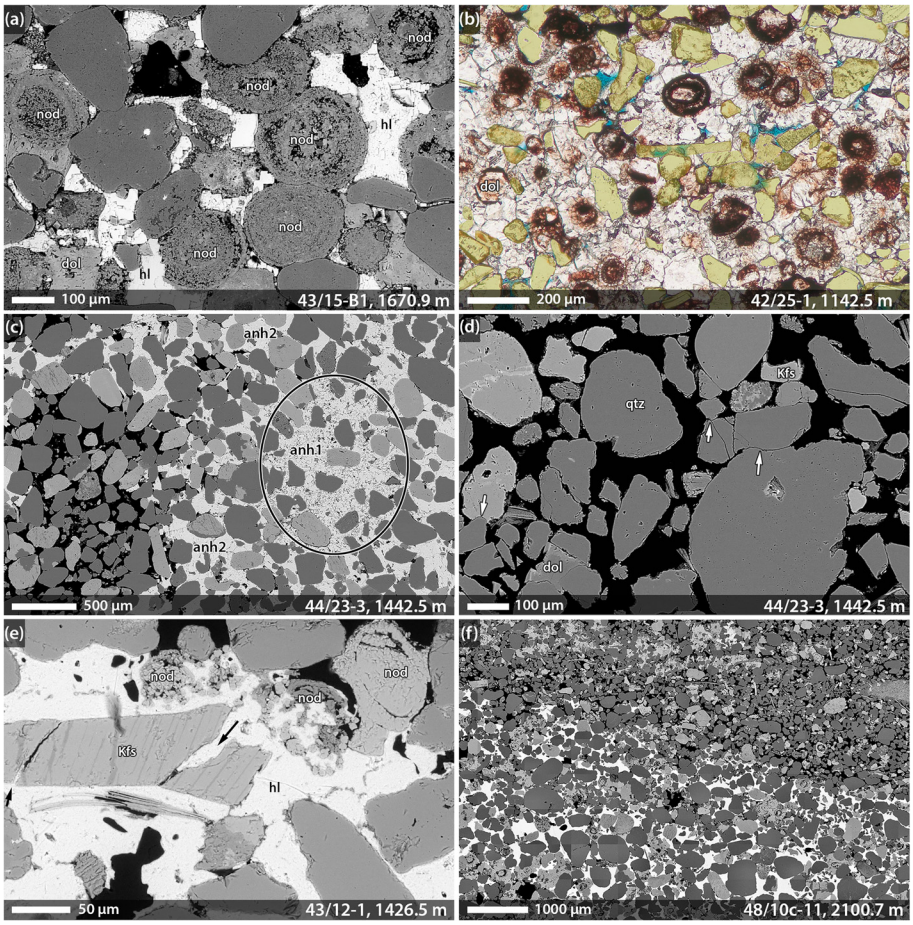

Fig. 3. Summary petrographical plate showing the main textural and diagenetic features of the BSF (Rushton *et al.* 2023). Well and depth are identified per image. (**a**) BSE showing dolomicritic nodules (nod) with well-defined concentric textures. Here they form a significant part of the framework and show evidence of compaction deformation at grain contact sites. Halite and coarser dolomite occlude post-compactional pore space (hl, halite; dol, dolomite). (**b**) Optical plain polarized light image from a millimetre-thick calcrete with abundant hematitic clay-defined nodules. The yellow AQM-derived overlay of detrital silicate grains highlights their widespread displacement by nodule-centred eodiagenetic calcite cement. Note the dolomite-replaced nodule (dol). (**c**) This BSE image shows texturally discrete forms of anhydrite. The encircled area contains a nodule of finely crystalline anhydrite (anh1) with an 'expanded' grain fabric suggesting pre-compaction formation with an element of displacive formation. The surrounding sandstone has a variably compacted texture and is cemented by poikilotopic anhydrite (anh2). Notched and embayed margins in the left of this field of view indicate that some anhydrite dissolution has occurred. (**d**) BSE image highlighting submillimetre-scale textural heterogeneity with 'floating' grains adjacent to sites displaying evidence of significant compaction (arrowed, concavo-convex and sutured grain contacts, and compaction-induced grain fracture) (qtz, quartz; Kfs, K-feldspar; dol, dolomite). (**e**) BSE image. Halite (hl) cement formed in compaction-induced fractures (arrows) and has also occluded intragranular micropores associated with some eodiagenetic nodules (nod). Notched, porous and embayed margins to halite are evidence of its partial dissolution. (**f**) A BSE image of a finely laminated, very-fine-, fine- and medium-grained sandstone in which halite preferentially cements the coarser-grained laminations.

replacement or dissolution – as described above. Therefore, petrographically calculated minus-cement primary porosities are subject to significant uncertainty. In most cases these calculated porosities are higher than theoretical values at the maximum burial depth (Table 3), using generic compaction curves for the North Sea from Ramm and Bjorlykke (1994) and maximum burial depths derived from Bulat and Stoker (1987). We note, however, that the expansive nature of the early carbonate and sulfate cements renders the use of generic burial curves suspect, and it is clear that a larger dataset with a broader representation is needed to properly characterize and understand the evolution of BSF porosity.

Paragenetic sequence

One of the main complicating factors in determining the paragenetic evolution of the BSF is that the diagenetic cements are multi-episode, with repeat periods of formation, replacement and dissolution for the main cements throughout the diagenetic sequence (carbonates, sulfates and halite). These are locally variable in content and extent, so that at any one site the evidence may only represent part of the full diagenetic history. This is reflected in the broad range of published models for the paragenetic evolution of the BSF.

Several eodiagenetic phases and textures recognized in this study point to evaporitic conditions being common throughout the deposition of both sandstones and interbedded mudstone laminations. Of particular note are the carbonate nodules, locally a major framework grain constituent, which we have identified as bearing concentric formation textures consistent with two formation mechanisms: (i) periodic *in situ* subsurface growth, interspersed with infiltered hematitic clay pellicle development, accompanied by (ii) local reworking (Rushton *et al.* 2023). Similar nodules have been recognized in the equivalent onshore Sherwood Sandstone Group (Burley 1984; Strong and Milodowski 1987; Plant *et al.* 1999; Monaghan *et al.* 2012). Apart from the recognition of calcrete horizons in the BSF (e.g. Muir *et al.* 1994; Blackbourn and Robertson 2014), these important framework constituents are poorly reported and described in most published petrographical studies for the UKSNS. Similarly, Muir *et al.* (1994) propose a shallow subsurface origin for some of the anhydrite based on Sr

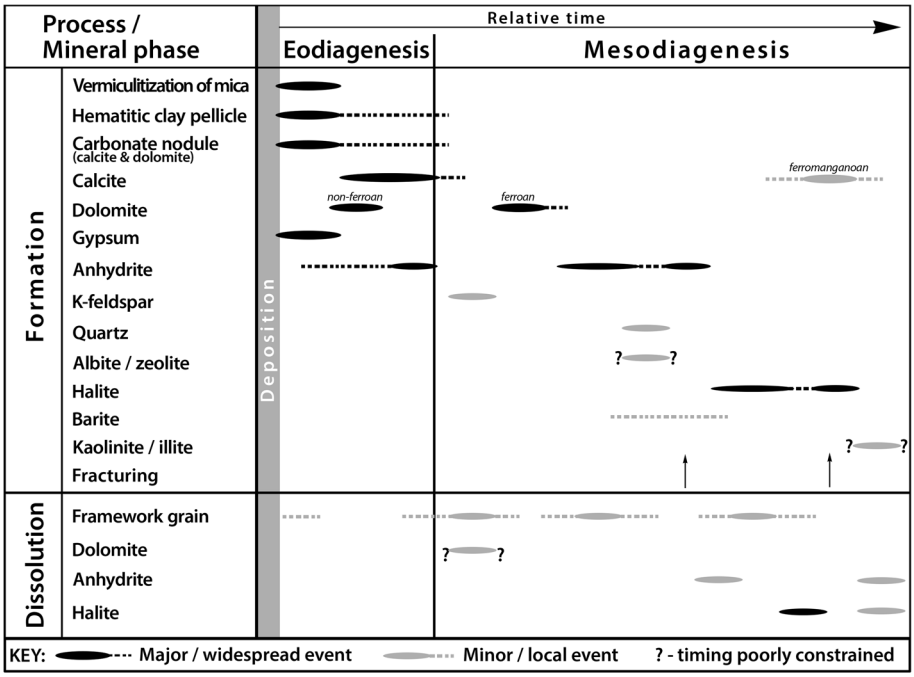

Fig. 4. Paragenetic sequence for the BSF in the UKSNS. Source: Rushton *et al.* (2023).

isotope data, which supports our interpretation of eodiagenetic anhydrite, which has formed both as a primary phase and through replacement of gypsum. Spain and Conrad (1997) also suggest early dolomite and anhydrite cementation controlled by palaeowater-table variability. Early anhydrite is also supported by anhydrite cementation excluding other cements (Purvis and Okkerman 1996) and resulting in low levels of compaction (Muir *et al.* 1994).

The timing of the halite cementation and the possibility of dissolution episodes has been variably interpreted in previous studies. Although halite has often been described as a late cement (Poroperm-Geochem Ltd 1987; Laier and Nielsen 1989; Van Bergen and de Leeuw 2001), in some cases it is described as forming, at least partially, post-hydrocarbon emplacement since halite appears inhibited in the gas leg (Poroperm-Geochem Ltd 1987; Ritchie and Pratsides 1993). These last observations are likely to be pre-gas emplacement local variations rather than a regional control; their deductions are contradicted by observations in this study that show halite also being well developed in some gas legs (wells 43/15-B1, 44/23-3 and 44/23a-10). In contrast, other authors have recognized halite as an early cement (Muir *et al.* 1994; Purvis and Okkerman 1996), with Purvis and Okkerman (1996) noting that the halite infilled pores with no other cements. Whilst our own observations place halite as a late phase *relative* to other diagenetic cements, our high minus-cement porosity values and the observations of widespread heterogeneous compaction textures (Fig. 3d) are consistent with the presence of widespread pore-filling cements that were developed prior to significant burial. Despite the different burial histories of sample sites (Bulat and Stoker 1987; Japsen 2000), we see this pattern of early and extensive cementation across most of the study area, except along the western edge (the samples from UK Block 41). This supports the inference that major cementation predated significant divergence in burial histories: i.e. before the Mid–Late Triassic onset of halokinesis and pre-Chalk uplift events.

Controls on cement distribution

We have observed a distribution of halite, and to a certain extent anhydrite, that is preferentially developed in coarser-grained sandstones. This has been observed by other authors, including in the Dutch Sector BSF equivalent (Poroperm-Geochem Ltd 1987; Ketter 1991; Purvis and Okkerman 1996), and its effect of occluding sandstone units with potentially the highest porosities and permeabilities has been termed 'reservoir quality inversion'. Most of the sandstones with abundant halite and all of the samples with complete halite cementation are fine-, medium- and coarse-grained, but not very fine, sandstone. The Lower Volpriehausen has the highest proportion of samples well-cemented by anhydrite and by halite due to its overall coarser grain sizes. However, not all of the coarser-grained sandstones are significantly halite cemented, showing that grain size does not solely control its distribution. The mesodiagenetic anhydrite is also locally preferentially developed in coarser-grained laminations. This inversion of reservoir quality occurs across much of the BSF, suggesting cementation resulting from an influx of brines during burial and/or uplift, rather than *in situ* evaporative formation. The existence of a permeability control on brine movement and cementation is implicit in this observation.

Furthermore, the presence of high levels of halite cement is only observed at and below a current burial depth of *c*. 1400 m within the Upper Volpriehausen (albeit constrained from a limited number of samples). Local variations in the degree of halite cementation show that current burial depth is not the only control on halite abundance; halite cementation is absent or incomplete for some samples at a burial depth of greater than 1400 m. However, it does seem to be a regional property, which may indicate additional dissolution has affected the formation above this depth. Different mechanisms for the removal of halite in structural highs have been proposed based on studies at the Endurance site. These include recent meteoric influx from the BSF outcrop at the crest of a salt diapir in the centre of the study area (Fig. 1: this would fit with our observation of reduced halite cementation above 1400 m), and thermohaline circulation associated with differential heating of the BSF through the underlying Zechstein salt and associated brine density variations (cf. Dingwall *et al.* 2013; Blackbourn and Robertson 2014; White Rose Project 2016).

Careful consideration is needed when attributing the origins of porosity created by halite dissolution. Some halite has formed in place of anhydrite, and both anhydrite and halite have locally replaced carbonates (both nodules and early cements). Consequently, high porosities identified where halite has been removed actually represent porosity after halite, sulfate and carbonate. Further, as the

nodular carbonates are largely framework grains, their replacement represents secondary porosity rather than restored primary porosity.

A striking feature of the BSF across the study area is the general absence of significant levels of diagenetic silicate cements, which may be attributed to pervasive early pore-filling cement. The only exceptions to this are samples from the Cleveland Basin at the western edge of the study area (near-shore well 41/18-1) where compaction textures are well developed and quartz cement is widespread. Whilst this area has experienced the greatest cumulative uplift (>2200 m: Day *et al.* 1981; Bulat and Stoker 1987; Japsen 2000), its maximum burial depth was also shallower than areas further east (Table 3). One suggestion is that at this basin margin the degree of early pore-filling cementation was much lower than in the rest of the area, allowing greater development of silicate overgrowths. However, it is also possible that the different degree of silicate cementation has arisen from other differences, particularly as many samples come from targeted potential reservoir structures, a consequence of site-specific halokinesis, therefore with potentially atypical thermal, fluid and structural conditions.

Timing of cement formation

The timing of significant pore-filling cements can commonly be determined from textural observations in the cemented areas (compaction and minus-cement porosity) combined with knowledge of regional and local burial histories. As previously noted, burial and uplift in the UKSNS since the deposition of the BSF results from regional tectonics and local halokinesis that has affected different parts of the basin to differing degrees. Continued burial post-BSF sedimentation through to the end of the Jurassic was followed by significant uplift into the Cretaceous, followed by further significant burial during which the Chalk was deposited. Subsequent further uplift occurred in the earliest Paleogene and also in the Neogene. Halokinesis is thought to have commenced during the Mid–Late Triassic and will have continued to create uplift patterns locally overprinting these regional trends. Consequently, straightforward burial histories cannot be applied over the whole study area. Simplifying, however, we can say that for most of the study area (but not all), maximum burial occurred during post-Chalk burial. Halokinetic-related uplift may have locally disrupted these regional trends. The inherent uncertainty related to the timing of halokinesis is a complicating factor in determining the timing of the main mesodiagenetic cements for the BSF relative to the episodes of burial and uplift, and therefore the controls on compaction.

Impacts on CO_2 storage

The principal diagenetic features and relative diagenetic chronology as relevant to fluid flow in the BSF are summarized schematically in Figure 5.

Layered cemented bands

Well test results from the proposed Endurance CO_2 storage site imply that vertical communication in the BSF is substantially reduced by the presence of numerous thin low-permeability baffles. The baffles extend laterally over distances of at least 50 m, with some extending for several hundreds of metres and others potentially more than 1 km in extent (BP 2021*b*). Cemented sandstone layers are interpreted to provide an important contribution to this vertical baffling in the BSF reservoir. Although cemented layers observed in core are generally of the order of about 10 cm or less in thickness, a several-metre-thick field-wide carbonate-cemented horizon was identified during appraisal activities at Endurance (BP 2021*c*). While this was interpreted during site appraisal studies to be associated with reworked ooids (Blackbourn and Robertson 2014; BP 2021*c*), spheroidal carbonate nodules observed in this study may imply an *in situ* origin for the observed ooid-like features.

Previous studies have applied numerical simulation methods to investigate the potential for CO_2 storage in parts of the BSF, incorporating cemented sandstone lithofacies in reservoir models (Williams *et al.* 2013; James *et al.* 2016). Both studies invoked the presence of a continuous and thin cemented sandstone horizon that had a potentially important impact on fluid flow within the reservoir. The continuous nature of the cemented horizon had the impact of dividing the BSF into an effective upper and lower reservoir division, with little or no hydraulic communication between. The presence of such a layer was shown to influence the distribution and behaviour of the simulated CO_2 plume by inhibiting gravity-driven (buoyancy) migration upwards towards the cap rock and potentially diverting CO_2 towards spill points by viscous forces during injection (Williams *et al.* 2013; James *et al.* 2016).

In a study of the multiphase flow characteristics of potential CO_2 storage reservoirs, including the BSF of the UKSNS, Reynolds *et al.* (2018) noted the importance of centimetre-scale heterogeneities on drainage and imbibition relative permeability and residual trapping. This implies that the observed dolocrete and calcrete layers are therefore likely to influence multiphase flow properties in addition to providing intrinsic permeability heterogeneity. Furthermore,

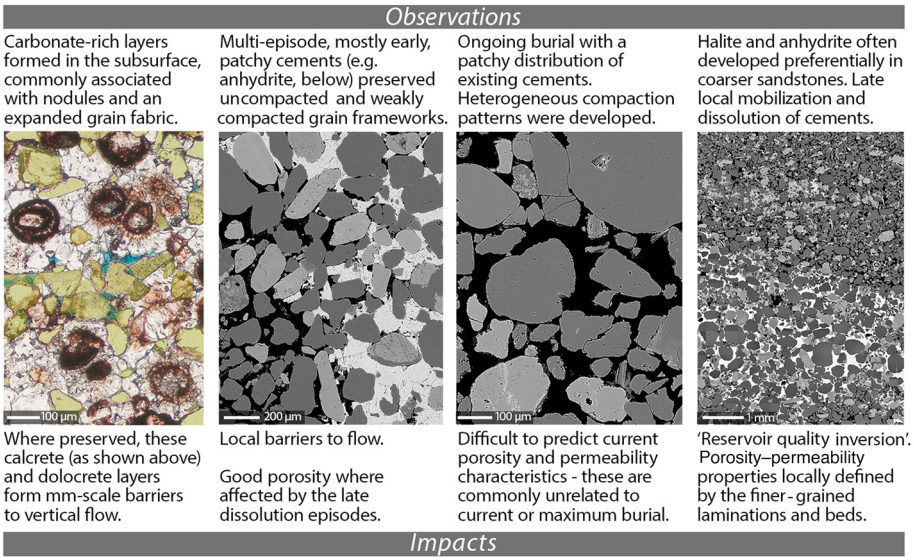

Fig. 5. A summary of the principal diagenetic features and relative diagenetic chronology derived from this study in the BSF.

Jackson and Krevor (2020) showed that small centimetre-scale capillary heterogeneities can be linked to enhanced rates of lateral plume migration during CO_2 storage. Where they occur in the BSF, rapid lateral CO_2 plume migration may occur beneath thin low-permeability cemented layers, providing a potential mechanism for unexpected migration towards structural spill points.

Impersistent or patchily distributed cemented layers will partially impede upwards migration of CO_2. This is likely to result in CO_2 contact with a greater reservoir surface area, resulting in improvements in microstructural, residual and dissolution trapping mechanisms (Al-Khdheeawi *et al.* 2017; Harris *et al.* 2021; Fang *et al.* 2023). By reducing the overall volume of CO_2 accumulating at the top of the reservoir in communication with the top seal, vertical baffling may provide a positive contribution to storage site integrity. Conversely, poor vertical connectivity may reduce injectivity and potentially lead to elevated pressure increase during injection.

Pervasive halite cement

Late-stage and pervasive halite cement is known to occlude porosity in parts of the BSF, with reduced porosities changing the acoustic properties sufficiently to result in a regionally extensive polarity phase reversal on seismic reflection data (Furnival *et al.* 2014; BP 2021*a*, *b*, *c*, 2022; Hollinsworth *et al.* 2022). The feature is particularly evident around the margins of the Endurance structure (Fig. 1). While the form of the phase-reversal polygon broadly conforms to structure, in places it directly crosses the present-day structural contours. This indicates that while the emplacement/dissolution processes responsible for the contrast are related to the halokinetic stage of basin development, they predate the present-day structural configuration. While analysis of a drill stem test in well 42/25d-3 indicates that average permeability within the Endurance structure is 270 mD, core-plug porosity–permeability transforms suggest permeabilities of the order of 30–50 mD outside of the structure and to the north of the phase-reversal polygon (BP 2021*b*). This is supported by post-production pressure measurements from the Esmond gas field, which have been used to infer reduced bulk reservoir permeabilities in the northern part of the BSF (Bentham *et al.* 2017). Consequently, CO_2 injection pressure can be expected to increase more rapidly in regions affected by pervasive late-stage halite cementation relative to regions where halite cements are less abundant. As observed in regional reservoir simulation studies, local pressure build-up will constrain the rate at which CO_2 can be stored in the BSF (Noy *et al.* 2012; Agada *et al.* 2017).

Elsewhere in the BSF, where significant halite cement is observed, it is restricted to specific intervals and preferentially affects coarser-grained sandstones. Although relatively few samples were available to this study, the observation that significant halite cement is only observed in samples at or below 1400 m depth suggests a depth control on the preservation of halite cement. This potentially supports the models invoked for dissolution of halite proposed to explain the seismic phase reversal highlighted by appraisal efforts at the Endurance site (Dingwall *et al.* 2013; Blackbourn and Robertson 2014; White Rose Project 2016). Further sampling and analyses would be required to ascertain if the 1400 m limit is consistent; however, it is worth highlighting that the seismic polarity reversal does not conform exactly to structure, and evidence for a diagenetic hardground contact surface is currently lacking.

Predictability of reservoir quality

Predicting reservoir quality is complicated by the long diagenetic history of the BSF, which comprises multiple episodes of cement formation, dissolution and replacement. Different fabrics appear to control flow in different parts of the reservoir, hence making simple predictions of flow behaviour challenging. Preferential cementation of coarser-grained sandstone by halite and/or anhydrite formed during mesodiagenesis leads to porosity inversion, where the porosity of coarser-grained units has become occluded. While common, this is not ubiquitous in coarser-grained units. Additionally, the carbonate nodules are commonly concentrated in finer-grained laminations, dictated by sedimentary structure; however, neither is this exclusive. While it is possible to identify some thicker cemented sandstone intervals using combinations of petrophysical logs, porosity occlusion by halite is particularly problematic to identify on standard geophysical logs. While combinations of logs such as density, sonic and photoelectric factor provide good indicators of lithology, aspects such as vertical scale and fluid fill (particularly gas) can often mask more subtle secondary lithological changes, attenuating what would otherwise be clear log responses. Moreover, water-soluble cements such as halite may not always be apparent through detailed examination of cores, depending on the methods of preservation and degrees of cleaning prior to study. Anhydrite, while less readily removed by poor core handling, can also adversely affect log-derived porosity interpretation as its relatively high density can lead to an underestimation of porosity. These factors can limit the ability to understand *in situ* downhole cementation from legacy well data. The complex diagenetic history, particularly the detachment of cement formation from burial-related processes, is also likely to impede efforts to derive porosity–depth trends for the BSF. One expected outcome of the abundant cementation, pre-maximum burial, including the preservation of eodiagenetic fabrics, is that BSF porosities may not exhibit a uniformly linear variation with maximum burial depth. This is supported by the observation of millimetre-scale heterogeneity in the degree of compaction, with areas of well-compacted framework grains immediately adjacent to areas with more open and expanded fabrics.

Conclusions

This study investigated the diagenetic controls on reservoir quality in the UKSNS BSF through petrographical analysis of 78 samples from 12 wells. The aim was to provide insights into the impact of diagenesis on reservoir characteristics as they relate to the ambition to use the BSF to store CO_2 captured from industrial processes. The following conclusions summarize the petrographical observations:

- In common with previous studies of the BSF, petrographical observations indicate terrestrial deposition in an arid to semi-arid environment dominated by fluvial processes with some input of aeolian grains.
- Diagenetic phases and cements are common to abundant through the BSF, marked by early (near-surface) carbonate and sulfate cements, with later sulfates and then halite. Some sandstones are completely cemented by diagenetic phases, while others have high porosities with negligible diagenetic cements.
- Carbonate nodules (calcite and dolomite) are an abundant framework grain constituent throughout the BSF and are most abundant in wells from the central to eastern parts of the study area (Quadrant 43 and Quadrant 44).
- While common framework positions of the carbonate nodules in sandstone fabrics might be taken as evidence of a purely detrital origin (i.e. as ooids), there is abundant and widespread evidence that they formed through both surface and shallow subsurface processes, potentially with several periods of development, shallow burial, mobilization and redeposition.
- The halite and anhydrite cements in their current distribution cannot have been the primary control on the degree of compaction in the BSF. The diagenetic model proposed

considers that the sandstones had abundant, but not complete, early cements that preserved shallow framework fabrics. As these cements were partial, compactional fabrics were created in the surrounding less- or non-cemented zones. Subsequent dissolution and replacement of some or all of the cement phases, notably the anhydrite and halite, post-maximum burial, has resulted in the widely recognized heterogeneous compaction fabric that does not correspond to current cement distributions. Since these phases have also partially replaced some of the framework carbonate nodules, their subsequent dissolution could also create an apparently uncompacted fabric.

One expected outcome of abundant, pre-maximum burial cementation is that BSF porosities may not define a simple linear variation with maximum burial depth. This is observed for petrographically calculated minus-cement primary porosities, where determined. They are, in most cases, similar to estimated theoretical porosities at the current burial depth. It is recognized that this inference is limited by the small sample set and high uncertainties in minus-cement determination due to the abundant diagenetic cement and complex sequence of carbonate nodule formation and replacement.

While the distribution of wells sampled across the northern part of the UKSNS has enabled the establishment of a basin-wide paragenetic model for the BSF, the sparse sampling limits the ability to provide conclusive evidence that would support predictions of reservoir quality distribution. Additional high-density sampling of BSF cores would be required to establish any spatial or depth dependence on pervasive halite and anhydrite cement. Given that acidic conditions arise from the dissolution of CO_2 in brine, the observation that carbonate nodules are present as abundant framework constituents also merits investigation of potential dissolution effects and their impact on the geomechanical integrity (potential compaction and porosity loss) of the BSF reservoir.

An additional limitation of the study is that most samples have come from legacy hydrocarbon industry boreholes that have targeted potential reservoir structures. Many of these structures resulted from halokinesis, which may have occurred differentially across the basin. As a result, individual structures may have experienced atypical thermal, fluid and structural conditions. Integrating petrographical observations with site-specific burial history studies may provide further insights into the causative mechanisms behind the post-burial diagenetic processes affecting the BSF.

Acknowledgements Sam Holloway is thanked for initiating early studies of BSF diagenesis at the British Geological Survey, and Lucy Abel is thanked for assistance in the preparation of Figures 1 and 2. We thank the reviewers for their constructive comments that improved the submission. This paper is published with the permission of the Executive Director, British Geological Survey (NERC, UKRI).

Author contributions **JCR**: conceptualization (equal), data curation (equal), formal analysis (lead), investigation (lead), methodology (lead), project administration (supporting), writing – original draft (equal), writing – review & editing (lead); **SH**: conceptualization (equal), formal analysis (supporting), funding acquisition (supporting), investigation (supporting), methodology (supporting), writing – original draft (supporting), writing – review & editing (supporting); **JP**: conceptualization (equal), writing – original draft (equal), writing – review & editing (supporting); **JW**: conceptualization (equal), data curation (equal), funding acquisition (lead), writing – original draft (supporting), writing – review & editing (supporting); **AEM**: formal analysis (supporting), investigation (supporting), methodology (supporting), writing – original draft (supporting), writing – review & editing (supporting).

Funding We acknowledge funding from the UK Carbon Capture and Storage Research Centre 2017 (EPSRC grant No. EP/P026214/1) and the Industrial Decarbonisation Research and Innovation Centre (EPSRC grant No. EP/V027050/1). The research also benefited from British Geological Survey National Capability funding from the Natural Environment Research Council (NERC).

Competing interests The authors declare that they have no known competing financial interests or personal relationships that could have appeared to influence the work reported in this paper.

Data availability The datasets generated during and/or analysed during the current study are not publicly available as they are part of an ongoing study but are available from the corresponding author on reasonable request.

References

Agada, S., Jackson, S. *et al*.. 2017. The impact of energy systems demands on pressure limited CO_2 storage in the Bunter Sandstone of the UK Southern North Sea. *International Journal of Greenhouse Gas Control*, **65**, 128–136, https://doi.org/10.1016/j.ijggc.2017.08.014

Al-Khdheeawi, E.A., Vialle, S., Barifcani, A., Sarmadivaleh, M. and Iglauer, S. 2017. Impact of reservoir wettability and heterogeneity in CO_2-plume migration and trapping capacity. *International Journal of Greenhouse Gas Control*, **58**, 142–158, https://doi.org/10.1016/j.ijggc.2017.01.012

Bentham, M., Mallows, T., Lowndes, J. and Green, A. 2014. CO_2 STORage Evaluation Database (CO_2 Stored). The UK's online storage atlas. *Energy Procedia*, **63**, 5103–5113, https://doi.org/10.1016/j.egypro.2014.11.540

Bentham, M., Williams, G., Vosper, H., Chadwick, A., Williams, J. and Kirk, K. 2017. Using pressure recovery at a depleted gas field to understand saline aquifer connectivity. *Energy Procedia*, **114**, 2906–2920, https://doi.org/10.1016/j.egypro.2014.11.540

Bifani, R. 1986. Esmond Gas Complex. *Geological Society, London, Special Publications*, **23**, 209–221, https://doi.org/10.1144/GSL.SP.1986.023.01.13

Blackbourn, G.A. and Robertson, L.F. 2014. *Sedimentology, Petrography and Burial History of the Cored Triassic Section in the National Grid Carbon Well 42/25d-3, UK North Sea*. Blackbourn Geoconsulting, Bo'ness, West Lothian, UK, https://ndr.ogauthority.co.uk/

BP 2021*a*. *Primary Store Geophysical Model & Report*. Key Knowledge Document NS051-SS-REP-000-00013, https://assets.publishing.service.gov.uk/media/6294fc4d8fa8f503921c150a/NS051-SS-REP-000-00013-Geophysical_Model___Report.pdf

BP 2021*b*. *Primary Store Dynamic Model & Report*. Key Knowledge Document NS051-SS-REP-000-00015, https://assets.publishing.service.gov.uk/media/6294fca0d3bf7f037097bdc7/NS051-SS-REP-000-00015-Dynamic_Model___Report.pdf

BP 2021*c*. *Primary Store Geological Model & Report*. Key Knowledge Document NS051-SS-REP-000-00014, https://assets.publishing.service.gov.uk/media/6294fc6cd3bf7f03667c656e/NS051-SS-REP-000-00014-Geological_Model___Report.pdf

BP 2022. *Alternative Stores and Notional Development Plan*. Key Knowledge Document NS051-SS-REP-000-0002, https://assets.publishing.service.gov.uk/media/6295281be90e070394dbc161/NS051-SS-REP-000-00022-Alt_Stores___Notional_Dev_Plan.pdf

Bulat, J. and Stoker, S.J. 1987. Uplift determination from interval velocity studies, UK southern North Sea. *In*: Brooks, J. and Glennie, K.W. (eds) *Proceedings of the 3rd Conference on Petroleum Geology of North West Europe*. Graham & Trotman, London, 293–305.

Burley, S.D. 1984. Patterns of diagenesis in the Sherwood Sandstone Group (Triassic), United Kingdom. *Clay Minerals*, **19**, 403–440, https://doi.org/10.1180/claymin.1984.019.3.11

Cameron, T.D.J., Crosby, A., Balson, P.S., Jeffery, D.H., Lott, G.K., Bulat, J. and Harrison, D.J. 1992. *The Geology of the Southern North Sea. United Kingdom Offshore Regional Report*. British Geological Survey and HMSO, London.

Coles, B. 1998. Doggerland: a speculative survey. *Proceedings of the Prehistoric Society*, **64**, 45–81, https://doi.org/10.1017/S0079497X00002176

Day, G.A., Cooper, B.A., Andersen, C., Burgers, W.F.J., Rønnevik, H.C. and Schoneich, H. 1981. Regional seismic structure maps of the North Sea. *In*: Hobson, G.D. and Illing, L.V. (eds) *Petroleum Geology of the Continental Shelf of North-West Europe*. Institute of Petroleum, London, 76–84.

Dingwall, S., Furnival, S., Wright, S. and Morrison, D. 2013. Integrated subsurface evaluation of a saline aquifer selected for CO_2 disposal. *In*: *75th EAGE Conference & Exhibition incorporating SPE EUROPEC 2013*. European Association of Geoscientists & Engineers (EAGE), Houten, The Netherlands, https://doi.org/10.3997/2214-4609.20130822

Doornenbal, H. and Stevenson, A. (eds) 2010. *Petroleum Geological Atlas of the Southern Permian Basin Area*. EAGE, Houten, The Netherlands.

Fang, X., Lv, Y., Yuan, C., Zhu, X., Guo, J., Liu, W. and Li, H. 2023. Effects of reservoir heterogeneity on CO_2 dissolution efficiency in randomly multi-layered formations. *Energies*, **16**, 5219, https://doi.org/10.3390/en16135219

Furnival, S., Wright, S., Dingwall, S., Bailey, P., Brown, A., Morrison, D. and De Silva, R. 2014. Subsurface characterisation of a saline aquifer cited for commercial scale CO_2 disposal. *Energy Procedia*, **63**, 4926–4936, https://doi.org/10.1016/j.egypro.2014.11.523

Gammer, D., Green, A., Holloway, S. and Smith, G. 2011. The Energy Technologies Institute's UK CO2 Storage Appraisal Project (UKSAP). Paper

SPE-148426 presented at the SPE Offshore Europe Oil and Gas Conference and Exhibition, 6–8 September 2011, Aberdeen, UK, https://doi.org/10.2118/148426-MS

Geluk, M.C. 2005. *Stratigraphy and Tectonics of Permo-Triassic Basins in the Netherlands and Surrounding Areas*. PhD thesis, Universiteit Utrecht, Utrecht, The Netherlands.

Geluk, M.C. and Röhling, H.-G. 1997. High-resolution sequence stratigraphy of the Lower Triassic 'Buntsandstein' in the Netherlands and northwestern Germany. *Geologie en Mijnbouw*, **76**, 227–246, https://doi.org/10.1023/A:1003062521373

Gluyas, J.G. and Bagudu, U. 2020. The Endurance CO_2 storage site, Blocks 42/25 and 43/21, UK North Sea. *Geological Society, London, Memoirs*, **52**, 163–171, https://doi.org/10.1144/M52-2019-47

Harris, C., Jackson, S.J., Benham, G.P., Krevor, S. and Muggeridge, A.H. 2021. The impact of heterogeneity on the capillary trapping of CO_2 in the Captain Sandstone. *International Journal of Greenhouse Gas Control*, **112**, https://doi.org/10.1016/j.ijggc.2021.103511

Hollinsworth, A.D., de Jonge-Anderson, I., Underhill, J.R. and Jamieson, R.J. 2022. Geological evaluation of suprasalt carbon storage opportunities in the Silverpit Basin, United Kingdom Southern North Sea. *AAPG Bulletin*, **106**, 1791–1825, https://doi.org/10.1306/03232221119

Holloway, S., Vincent, C.J., Bentham, M.S. and Kirk, K.L. 2006. Top-down and bottom-up estimates of CO_2 storage capacity in the UK sector of the Southern North Sea Basin. *Environmental Geoscience*, **13**, 74–81, https://doi.org/10.1306/eg.11080505015

Jackson, S.J. and Krevor, S. 2020. Small-scale capillary heterogeneity linked to rapid plume migration during CO_2 storage. *Geophysical Research Letters*, **47**, e2020GL088616, https://doi.org/10.1029/2020GL088616

James, A., Baines, S. and McCollough, S. 2016. *Strategic UK CCS Storage Appraisal – WP5A – Bunter Storage Development Plan*. Energy Technologies Institute, Loughborough, UK, https://doi.org/10.5286/UKERC.EDC.000267

Japsen, P. 2000. Investigation of multi-phase erosion using reconstructed shale trends based on sonic data. Sole Pit axis, North Sea. *Global and Planetary Change*, **24**, 189–210, https://doi.org/10.1016/S0921-8181(00)00008-4

Johnson, H., Warrington, G. and Stoker, S.J. 1994. Permian and Triassic of the southern North Sea. *In*: Knox, R.W.O'B. and Cordey, W.G. (eds) *Lithostratigraphic Nomenclature of the UK North Sea*. British Geological Survey for the UK Offshore Operators Association, Nottingham, UK, 33–51.

Ketter, F.J. 1991. The Esmond, Forbes and Gordon Fields, Blocks 43/8a, 43/13a, 43/15a, 43/20a, UK North Sea. *Geological Society, London, Memoirs*, **14**, 425–432, https://doi.org/10.1144/GSL.MEM.1991.014.01.53

Laier, T. and Nielsen, L.B. 1989. Cementing halite in Triassic Bunter Sandstone (Tønder, southwest Denmark) as a result of hyperfiltration of brines. *Chemical Geology*, **76**, 353–363, https://doi.org/10.1016/0009-2541(89)90103-4

McKie, T. and Williams, B. 2009. Triassic palaeogeography and fluvial dispersal across the northwest European Basins. *Geological Journal*, **44**, 711–741, https://doi.org/10.1002/gj.1201

Milodowski, A.E., Strong, G.E., Wilson, K.S., Holloway, S., Bath, A.H., Branch, C.H. and Spiro, B. 1987. *Diagenetic Influences in the Aquifer Properties of the Permo-Triassic Sandstones in the East Yorkshire and Lincolnshire Basin. Investigation of the Geothermal Potential of the UK*. British Geological Survey, Keyworth, Nottingham, UK.

Monaghan, A., Ford, J. *et al.*. 2012. 3D geological models of aquifer and seal rocks at analogue CO_2 storage sites in Lincolnshire and eastern Scotland, UK. *Proceedings of the Yorkshire Geological Society*, **59**, 53–76, https://doi.org/10.1144/pygs.59.1.289

Muir, R.O., Thirwall, M. and Walsh, J.N. 1994. *The Upper Buntsandstein in Well 49/6A-4. A Sedimentological and Geochemical Investigation of the Origins of the Cements*. Royal Holloway, University of London Report, https://ndr.ogauthority.co.uk/

Newell, A.J. 2018. Rifts, rivers and climate recovery: a new model for the Triassic of England. *Proceedings of the Geologists' Association*, **129**, 352–371, https://doi.org/10.1016/j.pgeola.2017.04.001

Noy, D.J., Holloway, S., Chadwick, R.A., Williams, J.D.O., Hannis, S.D. and Lahann, R.W. 2012. Modelling large-scale carbon dioxide injection into the Bunter Sandstone in the UK Southern North Sea. *International Journal of Greenhouse Gas Control*, **9**, 220–233, https://doi.org/10.1016/j.ijggc.2012.03.011

Paxton, S.T., Szabo, J.O., Ajdukiewicz, J.M. and Klimentidis, R.E. 2002. Construction of an intergranular volume compaction curve for evaluating and predicting compaction and porosity loss in rigid-grain sandstone reservoirs. *AAPG Bulletin*, **86**, 2047–2067, https://doi.org/10.1306/61EEDDFA-173E-11D7-8645000102C1865D

Pettijohn, F.J., Potter, O.E. and Seiver, R. 1987. *Sand and Sandstone*. Springer, New York.

Plant, J.A., Jones, D.G. and Haslam, H.W. (eds) 1999. *The Cheshire Basin: Evolution, Fluid Movement and Mineral Resources in a Permo-Triassic Rift Setting*. British Geological Survey, Keyworth, Nottingham, UK.

Poroperm-Geochem Ltd 1987. *Sedimentological and Petrological Analysis of Core from Wells 44/23-3 and 44/23-5*. CSX Oil and Gas (UK) Corp. Report 1956, https://ndr.ogauthority.co.uk/

Purvis, K. and Okkerman, J.A. 1996. Inversion of reservoir quality by early diagenesis: an example from the Triassic Buntsandstein, offshore the Netherlands. *In*: Rondeel, H.E., Batjes, D.A.J. and Nieuwenhuijs, W.H. (eds) *Geology of Gas and Oil Under the Netherlands*. Kluwer Academic, The Hague, The Netherlands, 179–189, https://doi.org/10.1007/978-94-009-0121-6_16

Ramm, M. and Bjorlykke, K. 1994. Porosity/depth trends in reservoir sandstones; assessing the quantitative effects of varying pore-pressure, temperature history and mineralogy, Norwegian Shelf data. *Clay Minerals*, **29**, 475–490, https://doi.org/10.1180/claymin.1994.029.4.07

Reynolds, C.A., Blunt, M.J. and Krevor, S. 2018. Multiphase flow characteristics of heterogeneous rocks from CO_2 storage reservoirs in the United Kingdom. *Water Resources Research*, **54**, 729–745, https://doi.org/10.1002/2017WR021651

Ritchie, J.S. and Pratsides, P. 1993. The Caister Fields, Block 44/23a, UK North Sea. *Geological Society, London, Petroleum Geology Conference Series*, **4**, 759–769, https://doi.org/10.1144/0040759

Rosenfeld, M A. 1949. Some aspects of porosity and cementation. *Producers Monthly*, **13**, 39–42.

Ruffell, A. and Hounslow, M. 2006. Triassic: seasonal rivers, dusty deserts and saline lakes. *In*: Rawson, P F. and Brenchley, P. (eds) *The Geology of England & Wales*. Geological Society, London, 295–325.

Rushton, J.C., Hannis, S. and Milodowski, A.E. 2023. *Petrography and Diagenesis of the Bunter Sandstone Formation in the UK Southern North Sea*. British Geological Survey Open Report OR/23/054. British Geological Survey, Keyworth, Nottingham, UK, https://nora.nerc.ac.uk/id/eprint/536777

Smith, D.J., Noy, D.J., Holloway, S. and Chadwick, R.A. 2011. The impact of boundary conditions on CO_2 storage capacity estimation in aquifers. *Energy Procedia*, **4**, 4828–4834, https://doi.org/10.1016/j.egypro.2011.02.449

Spain, J.D. and Conrad, C.P. 1997. Quantitative analysis of top-seal capacity: offshore Netherlands, southern North Sea. *Geologie en Mijnbouw*, **76**, 217–226, https://doi.org/10.1023/A:1003056609771

Strong, G.E. and Milodowski, A.E. 1987. Aspects of the diagenesis of the Sherwood Sandstones of the Wessex Basin and their influence on reservoir characteristics. *Geological Society, London, Special Publications*, **36**, 325–337, https://doi.org/10.1144/GSL.SP.1987.036.01.23

Testa, G. and Lugli, S. 2000. Gypsum-anhydrite transformations in Messinian evaporites of central Tuscany (Italy). *Sedimentary Geology*, **130**, 249–268, https://doi.org/10.1016/S0037-0738(99)00118-9

Underhill, J.R. 2003. The tectonic and stratigraphic framework of the United Kingdom's oil and gas fields. *Geological Society, London, Memoirs*, **20**, 17–59, https://doi.org/10.1144/GSL.MEM.2003.020.01.04

Underhill, J.R. 2009. Role of intrusion-induced salt mobility in controlling the formation of the enigmatic 'Silverpit Crater', UK Southern North Sea. *Petroleum Geoscience*, **15** 197–216, https://doi.org/10.1144/1354-079309-843

Van Bergen, F. and de Leeuw, C.S. 2001. Salt cementation of reservoir rocks near salt domes in the Netherlands North Sea area – a new mechanism. *In*: *63rd EAGE Conference & Exhibition*. European Association of Geoscientists & Engineers (EAGE), Houten, The Netherlands, https://doi.org/10.3997/2214-4609-pdb.15.P607

Van Hoorn, B. 1987. Structural evolution, timing and tectonic style of the Sole Pit inversion. *Tectonophysics*, **137**, 239–284, https://doi.org/10.1016/0040-1951(87)90322-2

Walker, J., Gaffney, V., Fitch, S., Muru, M., Fraser, A., Bates, M. and Bates, R. 2020. A great wave: the Storegga tsunami and the end of Doggerland? *Antiquity*, **94**, 1409–1425, https://doi.org/10.15184/aqy.2020.49

Walker, T.R., Waugh, B. and Grone, A.J. 1978. Diagenesis in first-cycle desert alluvium of Cenozoic age, southwestern United States and northwest Mexico. *Geological Society of America Bulletin*, **89**, 19–32, https://doi.org/10.1130/0016-7606(1978)89%3C19:DIFDAO%3E2.0.CO;2

Warren, J.K. 2006. *Evaporites. Sediments, Resources and Hydrocarbons*. Springer, Berlin.

Williams, J.D.O., Jin, M., Bentham, M., Pickup, G.E., Hannis, S.D. and Mackay, E.J. 2013. Modelling carbon dioxide storage within closed structures in the UK Bunter Sandstone Formation. *International Journal of Greenhouse Gas Control*, **18**, 38–50, https://doi.org/10.1016/j.ijggc.2013.06.015

White Rose Project 2016. *K40: Subsurface Geoscience and Production Chemistry Reports. Technical: Storage*. Department of Energy and Climate Change (DECC), London, https://assets.publishing.service.gov.uk/media/5a7f8d2440f0b62305b87d51/K40_Subsurface_Geoscience_and_Production_Chemistry.pdf

Ziegler, P.A. 1982. Triassic rifts and facies patterns in western and central Europe. *Geologische Rundschau*, **71**, 747–772, https://doi.org/10.1007/BF01821101